Magnetic doping of the golden cage cluster $M@Au_{16}^-$ (M=Fe,Co,Ni)

Lei-Ming Wang,[1] Jaeil Bai,[2] Anne Lechtken,[3] Wei Huang,[1] Detlef Schooss,[3,*] Manfred M. Kappes,[3,4] Xiao Cheng Zeng,[2,†] and Lai-Sheng Wang[1,‡]

[1]*Department of Physics, Washington State University, 2710 University Drive, Richland, Washington 99354, USA and Chemical and Materials Sciences Division, Pacific Northwest National Laboratory, MS K8-88, P.O. Box 999, Richland, Washington 99352, USA*

[2]*Department of Chemistry and Center for Materials and Nanoscience, University of Nebraska–Lincoln, Lincoln, Nebraska 68588, USA*

[3]*Institut für Nanotechnologie, Forschungszentrum Karlsruhe, Postfach 3640, 76021 Karlsruhe, Germany*

[4]*Institut für Physikalische Chemie, Universität Karlsruhe, Kaiserstraße 12, 76128 Karlsruhe, Germany*

(Received 19 December 2008; published 30 January 2009)

Structural, electronic, and magnetic properties of the golden cage doped with a transition-metal atom, MAu_{16}^- (M=Fe,Co,Ni), are investigated using trapped ion electron diffraction, photoelectron spectroscopy, and density-functional theory. The best agreement to experiment is obtained for endohedral $M@Au_{16}^-$ structures but with considerable distortions to the parent Au_{16}^- cage. $Fe@Au_{16}^-$ and $Co@Au_{16}^-$ are found to have similar structures with C_2 symmetry while a C_1 structure is obtained for $Ni@Au_{16}^-$. The 4*s* electrons are observed to transfer to the Au_{16} cage, whereas atomiclike magnetism due to the unpaired 3*d* electrons is retained for all the doped clusters.

DOI: 10.1103/PhysRevB.79.033413 PACS number(s): 36.40.Cg, 36.40.Mr, 61.48.−c

The local magnetic properties of dilute magnetic impurities in nonmagnetic hosts have been addressed with great experimental and theoretical efforts in the past decades.[1–7] Atomic clusters provide a unique medium for exploring local magnetism as the cluster size, the number of valence electrons, and the local structures can be readily controlled and varied.[8–13] In particular, a single magnetic atom trapped in a metallic cage would be an interesting system and an ideal molecular model for dilute magnetic alloys.[14–19] The Au_{16}^- cluster has been found recently to possess a hollow cage structure with a slightly distorted tetrahedral (T_d) symmetry,[20] which has a sufficiently large internal volume to encapsulate a foreign atom to form endohedral clusters. Several theoretical and experimental studies have been recently reported on doped Au_{16}^- clusters.[21–28] Both endohedral and exohedral dopings have been observed, and the structures of doped Au_{16}^- clusters are found to be determined by the nature of the dopant-Au interactions. Here we report a study on doping the Au_{16}^- cage with transition-metal atoms, MAu_{16}^- (M=Fe,Co,Ni). We found that the three magnetic atoms are all doped inside the golden cage but with significant distortions to the parent cage structure. The dopant atoms maintain their atomiclike *d* configurations in $M@Au_{16}$, while their 4*s* electrons can be viewed as transferred to the golden cage.

We use trapped ion electron diffraction (TIED), photoelectron spectroscopy (PES), and density-functional theory (DFT) calculations in the current study. The TIED technique probes the atomic structures of size-selected cluster ions.[29] Its potential has been demonstrated by a series of recent works on the structures of silver and gold cluster ions over a wide size range.[30–34] PES is a powerful technique to probe the electronic structure of size-selected clusters. The combination of these experimental techniques with DFT calculations affords a comprehensive understanding of the structural, electronic, and magnetic properties of the transition-metal-atom-doped golden cages.

The bimetallic cluster anions MAu_{16}^- (M=Fe,Co,Ni) were produced either by a magnetron sputtering source for TIED or by a laser vaporization source for PES using composite M/Au target disks. In the TIED experiment, about 10^5–10^6 size-selected cluster anions are stored in a radio frequency quadrupole ion trap and thermalized through collisions with a He buffer gas to a temperature of 100 ± 2 K. The ion cloud is then irradiated by an electron beam (40 keV, approximately 1–2 μA). Diffracted electrons from the clusters are detected by a phosphor screen assembly and integrated on a charge-coupled device (CCD) camera. The scattering picture is background corrected and converted into a modified molecular scattering intensity as a function of momentum transfer. This function is then compared to simulated scattering functions based on DFT candidate structures. A quantitative measure of the agreement between experimental and simulated scattering functions is expressed in a weighted profile factor R_w.[32] Further details of the experimental configuration and data analysis are given elsewhere.[32,33]

The PES experiment was performed using a magnetic-bottle PES apparatus equipped with a laser vaporization supersonic cluster source.[35] Negatively charged clusters were extracted from the cluster beam and analyzed using a time-of-flight mass spectrometer. The MAu_{16}^- clusters were selected and decelerated before being photodetached by a 193 nm laser beam from an ArF excimer laser. The photoelectron spectra were calibrated using the known spectrum of Au^-. The electron kinetic-energy resolution of the apparatus was $\Delta E/E \sim 2.5\%$.

In the theoretical study, we performed extensive structural searches using the basin-hopping algorithm[36] combined with DFT structural optimization.[37,38] The generalized-gradient approximation in the Perdew-Wang (PW91) functional form, implemented in the Vienna *ab initio* simulation package (VASP),[39] was used for the DFT calculations.[40] Specifically, the cutoff energy for the plane-wave expansion was 236 eV and the Brillouin zone was sampled with Γ point only. Periodic boundary conditions were employed in all three directions, whereas the dimension for the cubic supercell was $15 \times 15 \times 15$ Å^3. Typically, after 200–300 basin-hopping steps, a few tens of structurally distinct anion isomers were generated. These isomers were reoptimized using another DFT method, namely, the Perdew-Burke-Ernzerhof functional[41] with a scalar relativistic effective core potential and

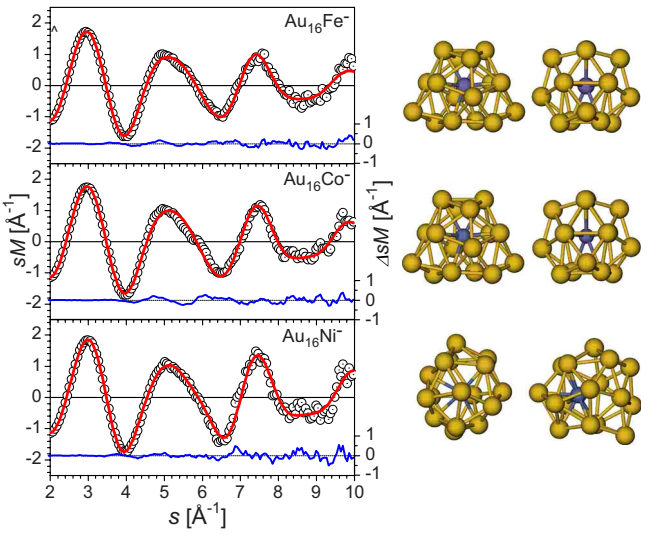

FIG. 1. (Color online) Modified experimental electron scattering functions (open circles) for $M\mathrm{Au}_{16}^-$ (M=Fe,Co,Ni) with the best fit [lines (red online)] using the structures shown on the right (two views rotated by 90°). The lower traces in each frame show the residuals.

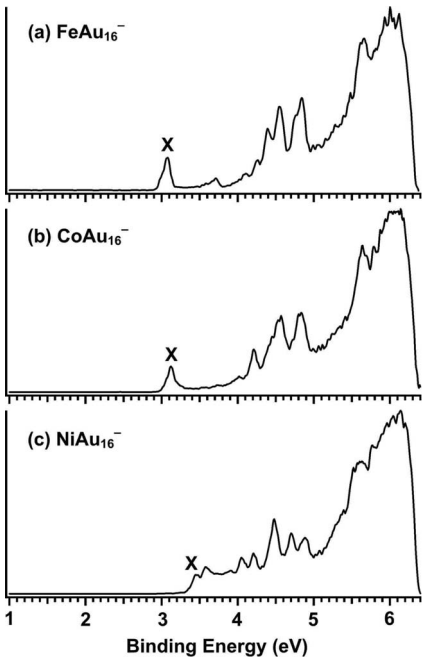

FIG. 2. Photoelectron spectra of $M\mathrm{Au}_{16}^-$ (M=Fe,Co,Ni) at 193 nm (6.424 eV).

LANL2DZ basis set implemented in the GAUSSIAN03 package.[42] Single-point energies of the corresponding neutral isomers in the anion geometries were then calculated to evaluate the first vertical detachment energy (VDE) of the anion isomers. The binding energies of deeper orbitals were added to the first VDE to give the VDEs of the excited states. Each calculated VDE was fitted with a Gaussian of width 0.04 eV to yield the simulated PES spectra.

Our global minimum search found many low-lying isomers close in energy and with subtle structural differences. Figure 1 displays the TIED data fitted using the best candidate structures for $M\mathrm{Au}_{16}^-$ (M=Fe,Co,Ni) that also agree well with the PES data, as will be discussed below. For FeAu_{16}^-, the lowest energy structure is of C_2 symmetry (Fig. 1), which is endohedral in nature but with some appreciable distortion to the parent tetrahedral (T_d) Au_{16}^- cage. Of all the low-lying structures the simulated scattering function of the C_2 isomer fits the TIED data best (R_w=2.7%). The endohedral structure with T_d symmetry shows a much larger R_w value (8.0%) and can be ruled out as a major contributor to the cluster ensemble probed. Nevertheless, a small contribution from the T_d-like structure is possible because a mixture fit by adding ~20% T_d isomer leads to a slight improvement in the R_w value (2.0%). The lowest energy structure found for CoAu_{16}^- is very similar to FeAu_{16}^-, i.e., a C_2 structure (Fig. 1), which is among the structures giving the best fit (R_w=3.3%) to the TIED data. However, several other low-lying endohedral structures can also fit the TIED data well. In particular, a C_1 structure (0.13 eV higher in energy) similar to NiAu_{16}^- (see below) gives a very good R_w value of 2.8%. Contributions from different isomers are also probable because mixtures of the C_2 or the C_1 structure with the T_d structure in the ratio of 0.7/0.3 or 0.8/0.2 lead to improved R_w values of 2.5% or 2.0%, respectively. However, we assign the C_2 isomer as the main contributor for CoAu_{16}^- because it is the lowest energy structure from our calculation and it also gives better agreement with our PES data (see below). For NiAu_{16}^-, the structure giving the best agreement between experimental and simulated scattering functions is a C_1 structure (R_w=2.4%), as shown in Fig. 1. The C_2 structure similar to FeAu_{16}^- or CoAu_{16}^- gives an R_w of 3.4% and a mixture fit of both does not significantly reduce the R_w value. Both structures are slightly higher lying isomers, 0.10 and 0.14 eV, respectively, above the lowest energy structure, which can be ruled out as a major component because of its high R_w value (9.1%). Again the tetrahedral cage structure (R_w=11%) can be ruled out as a major contributor.

The above structure assignments are corroborated and complemented by comparison between the experimental and simulated PES spectra. Figure 2 shows the experimental PES spectra of $M\mathrm{Au}_{16}^-$ (M=Fe,Co,Ni) at 193 nm. The spectra of FeAu_{16}^- and CoAu_{16}^- are similar, both featuring a low binding energy peak at ~3 eV (X) followed by an energy gap, a group of well-resolved peaks between 4 and 5 eV, and more congested Au 5d band beyond 5.5 eV. The spectrum of NiAu_{16}^- is very different and much more congested in the low binding energy range compared to that of FeAu_{16}^- and CoAu_{16}^-, suggesting that the structure of NiAu_{16}^- may also be very different as born out from the above comparison of TIED and DFT calculations. The PES spectra all seem to contain weak diffuse signals, more clearly in the cases of FeAu_{16}^- and CoAu_{16}^- following the X band [Figs. 2(a) and 2(b)], which may come from weakly populated isomers consistent with the TIED data. The first VDE for $M\mathrm{Au}_{16}^-$ is given in Table I.

It is informative to compare the current PES data with those of CuAu_{16}^- and ZnAu_{16}^-.[23,28] Both Cu and Zn have a closed 3d shell and the doped clusters possess endohedral structures with little distortion to the parent golden cage. $\mathrm{Cu@Au}_{16}^-$ is a closed-shell 18-electron system, in which the Cu 4s electron is transferred to the gold cage and it can be

TABLE I. The experimental vertical detachment energies (VDE) of $M\mathrm{Au}_{16}^{-}$ (M=Fe,Co,Ni) compared to calculated values.

	VDE (eV)	
	Expt.	Theor.
FeAu_{16}^{-} (C_2)	3.07 ± 0.03	3.08
CoAu_{16}^{-} (C_2)	3.11 ± 0.03	3.07
NiAu_{16}^{-} (C_1)	3.46 ± 0.04	3.51

viewed as $\mathrm{Cu}^{+} @ \mathrm{Au}_{16}^{2-}$.[23] The low binding energy range of its PES spectrum between 4 and 5 eV consists of a characteristic three-peak feature due to the t_2 and e valence molecular orbitals in the T_d cluster.[21] $\mathrm{Zn} @ \mathrm{Au}_{16}^{-}$ is a 19-electron system, in which the two 4s electrons of Zn are transferred to the golden cage. The extra electron in the anion enters a new electron shell, resulting in a low binding energy feature much separated from the three-peak feature derived from the t_2 and e orbitals. The PES spectra of FeAu_{16}^{-} and CoAu_{16}^{-} are reminiscent of the $\mathrm{Zn} @ \mathrm{Au}_{16}^{-}$ spectrum. In particular, the low binding energy peak (X) and the ensuring energy gap are very similar to what was observed in the spectrum of $\mathrm{Zn} @ \mathrm{Au}_{16}^{-}$, suggesting that the two 4s electrons of Fe($3d^6 4s^2$) and Co($3d^7 4s^2$) are also transferred to the golden cage and the extra electron in the anion enters in a new electron shell on the golden cage. The more complex spectral features between 4 and 5 eV suggest structural distortions to the parent cage, as well as possible contributions from the open 3d shell. The more complex PES spectrum of NiAu_{16}^{-} suggests a much more significant distortion to the parent gold cage. In particular, the missing low binding energy peak [Fig. 2(c)] implies that the extra electron in the NiAu_{16}^{-} anion enters a 3d orbital rather than a new shell on the gold cage, most likely due to the fact that in Ni the $3d^8 4s^2$ and $3d^9 4s^1$ configurations are nearly degenerate. All the above PES observations are consistent with the structural information derived from the TIED data.

The simulated PES spectra for $M @ \mathrm{Au}_{16}^{-}$ (Fig. 3) support the above interpretations and allow a better understanding of the experimental data. For FeAu_{16}^{-}, among several low-lying isomers, the simulated spectrum of the C_2 structure [Fig. 3(a)] agrees best with the experimental spectrum. Specifically, the weak peak observed at ~3.7 eV [Fig. 2(a)] in the gap region is well reproduced in the simulated spectrum by an Fe 3d derived band [Fig. 3(a)]. The first detachment band is indeed due to a Au 6s/p type orbital [also see the inset of Fig. 3(a)], similar to that in $\mathrm{Zn} @ \mathrm{Au}_{16}^{-}$. For CoAu_{16}^{-}, several low-lying isomers give similar simulated spectra, but the C_2 structure [Fig. 3(b)] gives the best overall fit to the experimental PES data. Similar to $\mathrm{Fe} @ \mathrm{Au}_{16}^{-}$ and $\mathrm{Zn} @ \mathrm{Au}_{16}^{-}$, the first PES feature in CoAu_{16}^{-} is also due to a Au 6s/p derived orbital [see the inset of Fig. 3(b)]. For NiAu_{16}^{-}, only the C_1 structure gives a simulated spectrum [Fig. 3(c)], which agrees well with the experiment, validating the TIED structural assignment. Importantly, the first detachment feature from NiAu_{16}^{-} indeed comes from a Ni 3d derived orbital, as shown in the inset of Fig. 3(c). The calculated first VDE is also in good agreement with the experimental data, as compared in Table I. Overall, the comparison of the simulated and experimental PES results lends considerable further support to the structures obtained for the three transition-metal-doped golden cages. The transition-metal dopants are clearly endohedral in nature, albeit the parent golden cage is significantly distorted, in particular, in the case of Ni.

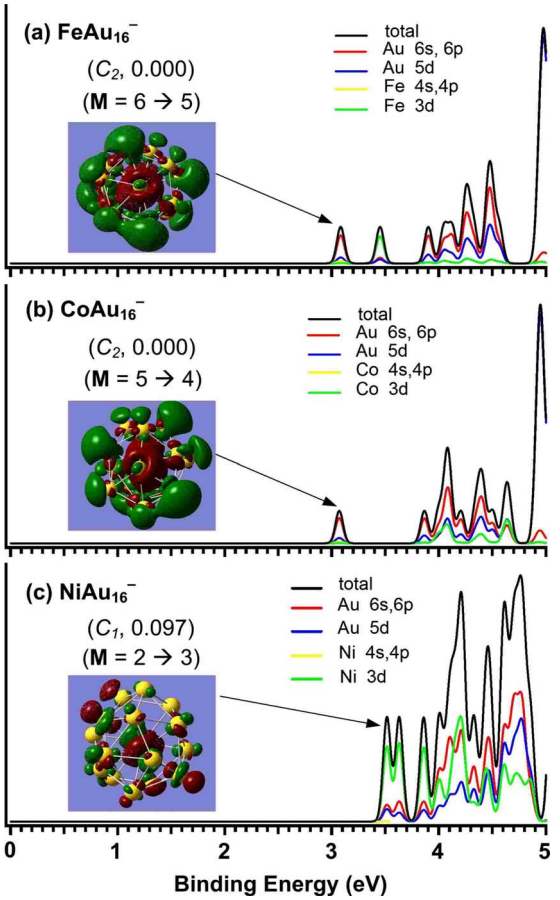

FIG. 3. (Color online) Simulated photoelectron spectra of $M\mathrm{Au}_{16}^{-}$ (M=Fe,Co,Ni) for the structures shown in Fig. 1. The symmetry and relative energy (in eV) are given in the parentheses. **M** denotes the spin multiplicity from the anion to the neutral. The inset shows the highest occupied molecular orbital. Contributions from different atomic orbitals to the density of states are also shown.

Previous studies show that the dopant-Au interactions are critical in determining the structures of the doped golden cages. Cu and Zn, which have closed 3d shells, primarily donate their 4s electrons to the cage, forming charge-transfer complexes with very little distortions to the cage.[23,28] Dopants, such as Si or W, have strong interactions with Au and they distort the golden cages and form other new types of structures.[24–26] The open 3d shells for Fe, Co, and Ni suggest that they may have more significant interactions with Au, leading to the observed structural distortions in the doped $M @ \mathrm{Au}_{16}^{-}$ clusters. Indeed, the decomposed density-of-states spectra in Fig. 3 show that the 3d orbitals of the dopant atoms have considerable hybridization with the host golden cage. This is particularly pronounced for $\mathrm{Ni} @ \mathrm{Au}_{16}^{-}$, consistent with its much distorted C_1 structure, in which the Ni atom appears to move to one side of the cage and interacts with fewer Au atoms (Fig. 1).

Interestingly, although there is considerable interaction between the transition-metal atoms and the host gold cage, the 3*d* states of the dopant atoms remain largely localized and the atomiclike magnetism is maintained in the doped clusters. We found that $Fe@Au_{16}^-$ ($\mathbf{M}=6$) and $Co@Au_{16}^-$ ($\mathbf{M}=5$) have high spins, while $Ni@Au_{16}^-$ has a lower spin ($\mathbf{M}=2$), consistent with the stronger Ni-cage interactions. Mulliken atomic spin density analyses show that the spin densities are mainly located on the central dopant atom for all three doped clusters. The bonding in the doped cluster anions can be viewed as an Au_{16}^{3-} interacting with a Fe^{2+}/Co^{2+} core or Au_{16}^{2-} interacting with a Ni^+ core. The neutral $M@Au_{16}$ clusters can all be described as $M^{2+}@Au_{16}^{2-}$ (M=Fe,Co,Ni), where the two 4*s* electrons are transferred to the cage and the dopant possesses d^6, d^7, and d^8 valence configurations, respectively, exactly like that in the atoms. Thus, the current work shows that the Au_{16} hollow cage provides a much more flexible host to protect the spins of the dopant atom. We anticipate that many other transition-metal atoms may be doped into the golden cage and maintain their local magnetic moments, forming a new class of endohedral golden cage clusters with varying magnetic properties.

The PES work was supported by NSF (Grant No. CHE-0749496) and performed at EMSL, a national scientific user facility sponsored by DOE's Office of Biological and Environmental Research and located at Pacific Northwest National Laboratory, operated for DOE by Battelle. The theoretical work was supported by grants from NSF (CHE, CMMI, MRSEC), and the Nebraska Research Initiative. The TIED work was supported by the Forschungszentrum Karlsruhe and the DFG, as administered through the Center for Functional Nanostructures.

*detlef.schooss@int.fzk.de
†xczeng@phase2.unl.edu
‡ls.wang@pnl.gov

[1] D. Riegel, L. Büermann, K. D. Gross, M. Luszik-Bhadra, and S. N. Mishra, Phys. Rev. Lett. **62**, 316 (1989).
[2] R. Kowallik, H. H. Bertschat, K. Biedermann, H. Haas, W. Müller, B. Spellmeyer, and W. D. Zeitz, Phys. Rev. Lett. **63**, 434 (1989).
[3] P. W. Anderson, Phys. Rev. **124**, 41 (1961).
[4] J. Kondo, in *Solid State Physics*, edited by F. Seitz, D. Turnbull, and H. Ehrenreich (Academic, New York, 1969), Vol. 23.
[5] P. Blaha and J. Callaway, Phys. Rev. B **33**, 1706 (1986).
[6] D. D. Vvedensky, M. E. Eberhart, and M. E. McHenry, Phys. Rev. B **35**, 2061 (1987).
[7] D. Guenzburger and D. E. Ellis, Phys. Rev. Lett. **67**, 3832 (1991).
[8] F. Liu, S. N. Khanna, and P. Jena, Phys. Rev. B **43**, 8179 (1991).
[9] I. M. L. Billas, A. Chatelain, and W. A. de Heer, Science **265**, 1682 (1994).
[10] S. E. Apsel, J. W. Emmert, J. Deng, and L. A. Bloomfield, Phys. Rev. Lett. **76**, 1441 (1996).
[11] G. M. Pastor, R. Hirsch, and B. Muhlschlegel, Phys. Rev. Lett. **72**, 3879 (1994).
[12] M. B. Knickelbein, Phys. Rev. Lett. **86**, 5255 (2001).
[13] M. Moseler, H. Hakkinen, and U. Landman, Phys. Rev. Lett. **89**, 176103 (2002).
[14] E. Janssens, S. Neukermans, H. M. T. Nguyen, M. T. Nguyen, and P. Lievens, Phys. Rev. Lett. **94**, 113401 (2005).
[15] Q. Sun, X. G. Gong, Q. Q. Zheng, D. Y. Sun, and G. H. Wang, Phys. Rev. B **54**, 10896 (1996).
[16] A. Pramann, A. Nakajima, and K. Kaya, J. Chem. Phys. **115**, 5404 (2001).
[17] S. N. Khanna, B. K. Rao, and P. Jena, Phys. Rev. Lett. **89**, 016803 (2002).
[18] W. Zheng, J. M. Nilles, D. Radisic, and K. H. Bowen, J. Chem. Phys. **122**, 071101 (2005).
[19] K. Tono, A. Terasaki, T. Ohta, and T. Kondow, Chem. Phys. Lett. **449**, 276 (2007).
[20] S. Bulusu, X. Li, L. S. Wang, and X. C. Zeng, Proc. Natl. Acad. Sci. U.S.A. **103**, 8326 (2006).
[21] M. Walter and H. Hakkinen, Phys. Chem. Chem. Phys. **8**, 5407 (2006).
[22] Y. Gao, S. Bulusu, and X. C. Zeng, ChemPhysChem **7**, 2275 (2006).
[23] L. M. Wang, S. Bulusu, H. J. Zhai, X. C. Zeng, and L. S. Wang, Angew. Chem., Int. Ed. **46**, 2915 (2007).
[24] L. M. Wang, S. Bulusu, W. Huang, R. Pal, L. S. Wang, and X. C. Zeng, J. Am. Chem. Soc. **129**, 15136 (2007).
[25] Q. Sun, Q. Wang, G. Chen, and P. Jena, J. Chem. Phys. **127**, 214706 (2007).
[26] Q. Sun, Q. Wang, P. Jena, and Y. Kawazoe, ACS Nano **2**, 341 (2008).
[27] W. Fa and J. M. Dong, J. Chem. Phys. **128**, 144307 (2008).
[28] L. M. Wang, R. Pal, W. Huang, X. C. Zeng, and L. S. Wang, J. Chem. Phys. (to be published).
[29] M. Maier-Borst, D. B. Cameron, M. Rokni, and J. H. Parks, Phys. Rev. A **59**, R3162 (1999).
[30] X. Xing, R. M. Danell, I. L. Garzon, K. Michaelian, M. M. Burns, and J. H. Parks, Phys. Rev. B **72**, 081405(R) (2005).
[31] X. P. Xing, B. Yoon, U. Landman, and J. H. Parks, Phys. Rev. B **74**, 165423 (2006).
[32] D. Schooss, M. N. Blom, and J. H. Parks, B. v. Issendorff, H. Haberland, and M. M. Kappes, Nano Lett. **5**, 1972 (2005).
[33] M. N. Blom, D. Schooss, J. Stairs, and M. M. Kappes, J. Chem. Phys. **124**, 244308 (2006).
[34] M. P. Johansson, A. Lechtken, D. Schooss, M. M. Kappes, and F. Furche, Phys. Rev. A **77**, 053202 (2008).
[35] L. S. Wang, H. S. Cheng, and J. W. Fan, J. Chem. Phys. **102**, 9480 (1995).
[36] D. J. Wales and H. A. Scheraga, Science **285**, 1368 (1999).
[37] S. Yoo and X. C. Zeng, J. Chem. Phys. **119**, 1442 (2003).
[38] S. Yoo and X. C. Zeng, Angew. Chem., Int. Ed. **44**, 1491 (2005).
[39] J. P. Perdew and Y. Wang, Phys. Rev. B **45**, 13244 (1992).
[40] G. Kresse and J. Hafner, Phys. Rev. B **47**, 558 (1993).
[41] J. P. Perdew, K. Burke, and M. Ernzerhof, Phys. Rev. Lett. **77**, 3865 (1996).
[42] M. J. Frisch *et al.*, GAUSSIAN03, Revision C.02, Gaussian, Inc., Wallingford, CT, 2004.